ELSEVIER

Journal of Wind Engineering
and Industrial Aerodynamics 85 (2000) 163–176

JOURNAL OF wind engineering AND industrial aerodynamics

www.elsevier.com/locate/jweia

The microscale model MIMO: development and assessment

J. Ehrhard[a,*], I.A. Khatib[a], C. Winkler[a], R. Kunz[a], N. Moussiopoulos[b], G. Ernst[a]

[a]*Institut für Technische Thermodynamik, Universität Karlsruhe, D-76128 Karlsruhe, Germany*
[b]*Laboratory of Heat Transfer and Environmental Engineering, Aristotle University Thessaloniki, GR-54006 Thessaloniki, Greece*

Abstract

The numerical model MIMO is a three-dimensional model for simulating microscale wind flow and dispersion of pollutants in built-up areas. It solves the Reynolds averaged conservation equations for mass, momentum and energy. Additional transport equations for humidity, liquid water content and passive pollutants can be solved. The Reynolds stresses and turbulent fluxes of scalar quantities can be calculated by several linear and nonlinear turbulence models. A staggered grid arrangement is used and coordinate transformation is applied to allow non-equidistant meshsize in all three dimensions in order to achieve a high resolution near the ground and near obstacles. The model was validated for a variety of test cases and it was applied successfully to air pollution problems.

Keywords: Urban atmosphere; Pollutant dispersion; Turbulence modeling; Numerical simulation; Coupling

1. Introduction

The increasing interest in the prediction of wind flow and pollutant dispersion over built-up areas and major advances in computer technologies have led to the development of efficient numerical models as an alternative or complementary approach to laboratory and field experiments. The microscale model MIMO [1] was developed at the Institut für Technische Thermodynamik on the basis of the non-hydrostatic

* Corresponding author. Present address: ABB ALSTOM POWER Technology Ltd., CH-5405 Baden-Dättwil, Switzerland. Tel.: +41-56-486-70-04; fax: +41-56-486-73-18.
E-mail address: jan.ehrhard@ch.abb.com (J. Ehrhard)

0167-6105/00/$ - see front matter
PII: S0167-6105(99)00137-3

mesoscale model MEMO [2,3]. It includes several linear and nonlinear eddy-viscosity turbulence models, which describe the production of turbulent kinetic energy due to shear stresses and vertical temperature gradients. To study dispersion processes transport equations for passive pollutants can be solved. The system of partial differential equations is discretized on a staggered grid and solved numerically.

The governing equations, the solution procedure and the formulation of initial and boundary conditions are described in Section 2. In Section 3 the coupling of the model MIMO to the mesoscale model MEMO, an approach to simulate scale interaction, is presented. Examples of the model predictions and comparisons with results from measurements are shown in Section 4.

2. Model equations and numerical solution

2.1. Governing equations

The model MIMO solves the conservation equations for mass, momentum, energy and other scalar quantities such as the humidity or the concentration of passive pollutants. According to Reynolds [4] the instantaneous value of a quantity $\tilde{\Phi}$ is split into a mean part Φ and a fluctuating part ϕ. In Table 1 the time averaged conservation equations for mass, momentum, energy and other scalar quantities are given in a general form, which consists of terms describing the temporal derivative, the advection, the diffusion and source terms. U_i is the mean velocity and x_i are the Cartesian co-ordinates. The energy equation is formulated employing the potential temperature θ defined as

$$\theta = T \cdot \left(\frac{p_0}{p}\right)^{R_L/c_p} \tag{1}$$

with the temperature T, the pressure p and the reference pressure $p_0 (= 10^5$ Pa) at ground level.

The mean state is assumed to be in hydrostatic equilibrium, i.e., $\partial p/\partial z = -\rho g$. Usually the density fluctuations ρ' are small compared to the mean density ρ_0. Introducing the assumption $\rho' \ll \rho_0$ into the conservation equation for momentum yields the simplified equation

$$\frac{\partial(\rho_0 U_i)}{\partial t} + \frac{\partial(\rho_0 U_i U_j)}{\partial x_j} = -\rho' g_i - \frac{\partial p}{\partial x_i} - \frac{\partial(\rho_0 \overline{u_i u_j})}{\partial x_j}, \tag{2}$$

where density variations in the inertia term are neglected, but retained in the buoyancy term (Boussinesq approximation).

2.2. Turbulence modeling

Numerical modeling of turbulence often plays a crucial role in providing accurate microscale wind fields, which are necessary to reliably predict transport and dispersion of pollutants in the vicinity of buildings.

To solve the conservation equations it is necessary to model the Reynolds stresses $\overline{u_i u_j}$ which arise from the averaging of the nonlinear transport equations for momentum. The most common turbulence models are based on the eddy viscosity hypothesis by Boussinesq which states that the Reynolds stresses $\tau_{ij} \equiv -\rho \cdot \overline{u_i u_j}$ are proportional to the mean strain rate S_{ij}:

$$\tau_{ij} = 2\mu_t S_{ij} - \frac{2}{3}\rho k \delta_{ij} \tag{3}$$

with

$$S_{ij} = 0.5 \cdot \left(\frac{\partial U_i}{\partial x_j} + \frac{\partial U_j}{\partial x_i} \right). \tag{4}$$

For brevity the Einstein summation convention was applied. The exchange coefficient or eddy viscosity μ_t which is defined by Eq. (3) is not a property of the fluid but a property of the flow field. The eddy viscosity is a characteristic quantity of the local turbulence and it is usually expressed in terms of the velocity and length scales of the turbulent motion.

Based on the desired accuracy and effort several turbulence models can be applied: The most simple turbulence model included in the microscale model MIMO is a one-equation turbulence model. It employs the kinetic energy of the turbulent fluctuations as the basis for the velocity scale which is necessary to compute the eddy viscosity. One-equation turbulence models are extremely simple, however they are incomplete as they relate the turbulence length scale to some typical flow dimension. In contrast, two-equation turbulence models provide an additional equation for the turbulence length scale or its equivalent and are thus complete, i.e., they can be used to determine a flow without prior knowledge of any flow details.

The standard k–ε two-equation turbulence model by Jones and Launder [5], hereafter labelled JL, determines the velocity and length scales of the turbulent motion by solving transport equations for the turbulent kinetic energy k ($= 0.5 \cdot \overline{u_i u_i}$) and the rate of its dissipation ε ($= k^{3/2}/L$). The proposed constants are $C_\mu = 0.09$, $C_{\varepsilon 1} = 1.44$, $C_{\varepsilon 2} = 1.92$, $\sigma_k = 1.0$ and $\sigma_\varepsilon = 1.3$. Besides the standard k–ε model the two-equation turbulence models by Kato and Launder [6] KL, Shih et al. [7] SH, Yakhot et al. [8] YA and Wilcox [9] WI are implemented in MIMO. Results obtained with these turbulence models are given in Section 4.1.

To account for buoyancy effects the production of turbulent kinetic energy and dissipation is augmented by an additional buoyancy term (see Table 1) depending on the Richardson number

$$\mathrm{Ri} = \frac{g}{\theta} \frac{\partial\theta/\partial z}{2S_{ij}^2}. \tag{5}$$

All the turbulence models mentioned above are based on the Boussinesq hypothesis given by Eq. (3). They are numerically robust and efficient, however they are known to

Table 1
Governing equations

General form of the conservation equation $\frac{\partial(\rho\Phi)}{\partial t}+\frac{\partial(\rho U_j\Phi)}{\partial x_j}=\frac{\partial}{\partial x_j}\left(\rho\Gamma\frac{\partial\Phi}{\partial x_j}\right)+S_\Phi$

Conservation of	Quantity Φ	Exchange coefficient Γ	Source/sink terms S_Φ
Mass	1	0	0
Momentum	U_i	μ_t	$-\frac{\partial p}{\partial x_i}-\frac{2}{3}\delta_{ij}\frac{\partial(\rho k)}{\partial x_j}\rho_0 g_i\frac{\theta}{\theta_0}$
Energy	θ	$\mu_t\cdot\sigma_\theta^{-1}$	$\rho Q\frac{\Delta h}{c_p}$
Turbulent kinetic energy	k	$\mu_t\cdot\sigma_k^{-1}$	$\tau_{ij}\frac{\partial U_i}{\partial x_j}\left(1-\frac{\mathrm{Ri}}{\sigma_\theta}\right)-\rho\varepsilon$
Dissipation rate	ε	$\mu_t\cdot\sigma_\varepsilon^{-1}$	$C_{\varepsilon1}\frac{\varepsilon}{k}\tau_{ij}\frac{\partial U_i}{\partial x_j}\left(1-\frac{C_{\varepsilon3}}{C_{\varepsilon1}}\frac{\mathrm{Ri}}{\sigma_\theta}\right)-C_{\varepsilon2}\rho\frac{\varepsilon^2}{k}$
Concentration	c	$\mu_t\cdot\sigma_\theta^{-1}$	0

have deficiencies in describing turbulent flows with body force effects arising from streamline curvature and Reynolds stress differences are not predicted correctly. Therefore, their application to highly complex flows can lead to considerable inaccuracies. These perceptions have led to the development of nonlinear stress–strain relationships that transcend the Boussinesq hypothesis, but are not considerably more complex in structure. A general constitutive relation for the Reynolds stresses under the assumption that the Reynolds stresses are dependent only on the mean velocity gradients and the characteristic scales of turbulence forms the basis of these models. Due to this general constitutive relation nonlinear effects in the modeling of the Reynolds stresses are taken into account. Therefore the capability to improve the prediction for example in recirculation regions where turbulence becomes highly anisotropic is inherent. Turbulence models based on a nonlinear stress–strain relationship are currently under investigation for the microscale model MIMO.

2.3. Solution procedure

The governing equations described in the previous section are solved numerically on a staggered grid (ARAKAWA C) by using a finite volume discretization procedure. Scalar quantities such as the pressure or the potential temperature are defined at the center of a cell while velocity components are specified at the center of the appropriate interfaces between two cells [10]. A co-ordinate transformation is applied in all dimensions to allow for higher resolution, e.g. near buildings or near the surface.

The conservation equation of mass is formulated in terms of the pressure yielding an elliptic differential equation. The discrete form of the elliptic equation is solved using a preconditioned conjugate gradient (CG) method. Preconditioning is

performed by a fast direct solution technique on the basis of the discrete fast Fourier transform (FFT) (see Ref. [11]).

For the numerical treatment of advective transport a 3-D second-order total-variation-diminishing (TVD) scheme is implemented which is based on the 1-D scheme proposed by Harten [12]. Furthermore a second-order flux-corrected transport (FCT) Adams–Bashforth scheme can be applied (Wortmann-Vierthaler and Moussiopoulos [13]). Both schemes are positive, transportive, conservative and they are characterized by a low level of numerical dissipation. Diffusion terms are treated by a second order central difference scheme.

2.4. Initial and boundary conditions

In the model MIMO two different possibilities for the initialization are included. The first possibility is to couple the microscale model MIMO with the mesoscale model MEMO (see Section 3). Alternatively the initial wind field can be calculated from measured data or by the power law

$$U(z) = U_{\mathrm{r}}\left(\frac{z}{z_{\mathrm{r}}}\right)^{\alpha}. \tag{6}$$

Herein U_{r} denotes the reference velocity at the corresponding height z_{r}. The exponent α depends on the thermal stratification. The temperature is initialized on the basis of measured profiles or by a constant gradient. Initialization of the pressure follows the thermal stratification according to the hydrostatic equation.

The boundary conditions are grouped with respect to the physical behaviour of the flow into lateral inflow and outflow boundaries, internal openings (where flow may enter or leave the domain), walls and planes of symmetry. At lateral inflow boundaries Dirichlet conditions are imposed for all main quantities except for the pressure, which must be of Neumann type. Homogeneous Neumann boundary conditions are imposed at lateral outflow boundaries for the main quantities. Internal openings are distinguished into easily penetrable obstacles, i.e., open factory buildings and planes emitting mass flux with an initial momentum like the exhaust of a stack or of a cooling tower. In the latter case the initial wind velocity is prescribed according to the mass flux at the emission exhaust. The flow inside an easily penetrable obstacle is resolved explicitly.

Wall boundary conditions prohibit fluid flow across the boundary surface. Additionally, the fluid is assumed to be at rest on the wall boundary surface (no-slip condition). The wall boundary condition for the velocity components is implemented by assuming a logarithmic profile in the region close to the wall (Launder and Spalding [14]). Based on this assumption, the value for the velocity gradient normal to the wall is determined. For the solution of the transport equation of turbulent kinetic energy next to solid walls it is assumed that the production rate of turbulent kinetic energy is equal to the dissipation rate. Dissipation at the first grid point adjacent to walls is set to its equilibrium value $\varepsilon = u_{\tau}^3/\kappa z$.

3. Coupling with the mesoscale model MEMO

Wind flow and pollutant dispersion over built-up areas are decisively influenced by the large-scale flow. Mesoscale wind flow systems like thermally induced valley winds, land-/sea-breeze circulations in costal areas or channelled flow along a valley usually govern the dispersion of pollutants in the surroundings of built-up areas. Inside urban areas the microscale flow is dominant. The microscale flow is, however, strongly affected by the mesoscale flow. For a realistic simulation of the microscale flow field proper boundary conditions have to be provided. For most applications no detailed measurements are available and therefore crude assumptions have to be made. In order to avoid this ambiguity a coupling method between the microscale model MIMO and a mesoscale model, e.g. the model MEMO, has been developed by Khatib [15]. The results of the mesoscale simulation serve as initial and boundary conditions for the microscale simulation. The coupling method enables to account for daytime variations of the wind speed and direction and the thermal stratification.

The coupling procedure consists of three elements: a three-dimensional interpolation, an adjustment for values within the surface layer and a formulation of the lateral boundary conditions to introduce the interpolated values into the microscale model at the lateral boundaries.

Fig. 1 shows the vertical structure of typical numerical grids of the models MEMO and MIMO. The domain sizes and resolutions differ considerably and therefore a three-dimensional interpolation must be applied. The microscale value $\hat{\Psi}$ is calculated by a weighted averaging of the eight surrounding mesoscale values Ψ (see Fig. 2):

$$\hat{\Psi} = \frac{1}{\sum_{i=1}^{8} V_i} \sum_{i=1}^{8} (V_i \cdot \Psi_i). \tag{7}$$

Due to its coarse resolution the mesoscale simulation gives only poor information about the vertical structure of the boundary layer adjacent to the ground. Therefore, the interpolated values are adjusted using similarity theory. The microscale wind profile in the surface layer is calculated using either the power law

$$U(z) = U_{\mathrm{sl}} \left(\frac{z}{z_{\mathrm{sl}}} \right)^{\mathrm{p}} \tag{8}$$

or the logarithmic law

$$U(z) = \frac{U_\tau}{\kappa} \left[\ln \left(\frac{z}{z_0} \right) + \phi_m \frac{z}{L} \right], \tag{9}$$

where U_{sl} is the mesoscale wind speed at the top of the surface layer z_{sl}, U_τ is the friction velocity, z_0 is the roughness height and L is the Monin-Obukhov length taken from the mesoscale simulation. The exponent p depends on thermal stability and κ is the von Kármán constant. The similarity function ϕ is calculated following Carson and Richards [16] and Hicks [17].

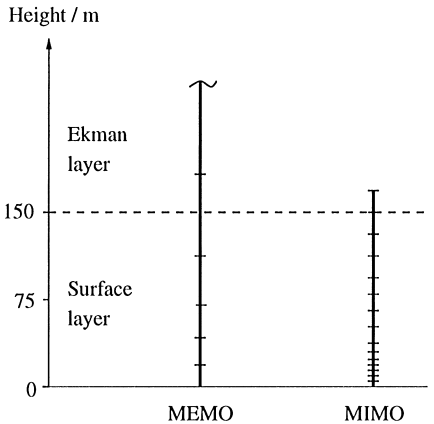

Fig. 1. Vertical structure of typical grids.

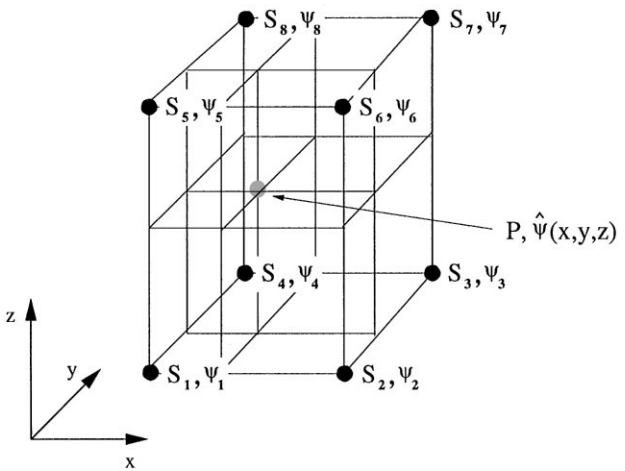

Fig. 2. Three-dimensional interpolation scheme.

The interpolated wind speed is introduced into the microscale model using an expanded radiation boundary condition proposed by Carpenter [18]. Further details are given by Khatib [15]. An example of a simulation performed with the coupled model is presented in Section 4.3.

4. Model application and validation

The microscale model MIMO was applied to simulate the flow around obstacles with simple geometries like a surface-mounted cube and a U-shaped building. The

results from these simulations were compared with results from wind tunnel experiments. Moreover, the model was applied successfully to predict plumes rising from cooling towers and dispersion of pollutants in built-up areas.

4.1. Flow over a surface-mounted cube

The rectangular cube is a very simple idealisation of a building. Although it is geometrically simple the corresponding flow is very complex with severe pressure gradients, streamline curvature and multiple, unsteady separation regions. Therefore, this simple type of flow already represents a formidable task for numerical models.

The flow over a cubic obstacle is characterized by an impingement region at the windward side of the cube. When approaching the cube the flow separates due to the increasing pressure. A main vortex develops which wraps around the cube into the wake. Because of its characteristic shape this structure is called a horse-shoe vortex. The flow separates at the upper edge of the cube forming a separation bubble. At the upper leeward edge of the cube the flow separates again and leads to a large recirculation region behind the cube which interacts with the horse-shoe vortex.

Numerical simulations of the flow around a cubic obstacle were carried out with the microscale model MIMO using five different two-equation turbulence models introduced in Section 2.2 (see also Table 2). A sketch of the model domain is shown in Fig. 3. The results obtained by MIMO were compared with the experimental results from Martinuzzi and Tropea [19].

The predicted height Z_T of the separation bubble on top of the cube (see Fig. 3) given in Table 2 is underestimated by the JL, KL and WI models whereas it is overestimated by the SH and YA models. The same tendency can be observed for the windward separation length X_F. The JL, KL and WI models underpredict this length whereas the SH and YA models overpredict it. The overprediction of X_F leads to a very large overprediction of the leeward reattachment length X_R. The recirculation region calculated by the KL model ($X_R/H = 2.92$) is larger than that of the JL model ($X_R/H = 2.50$). This is due to the fact that in the former model less turbulent kinetic energy is produced in the impingement region and therefore less turbulent kinetic energy is transported around the cube leading to a lower level of turbulent kinetic energy in the wake region. The modification aimed to improve the behaviour

Table 2
Characteristic lengths of the flow field

Type	Identity	Z_S/H	Z_T/H	X_F/H	X_R/H
k–ε	JL	0.65	0.09	0.67	2.50
k–ε	KL	0.67	0.14	0.75	2.92
k–ε	SH	0.68	0.19	1.02	3.26
k–ε	YA	0.69	0.21	0.98	3.18
k–ω	WI	0.66	0.06	0.76	2.31
Experiment	MT	0.65	0.17	0.84	1.66

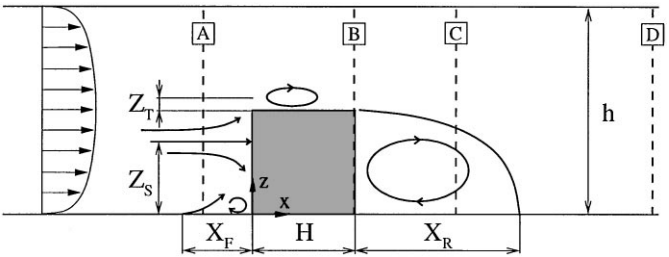

Fig. 3. Sketch of investigated cubic obstacle and location of vertical profiles.

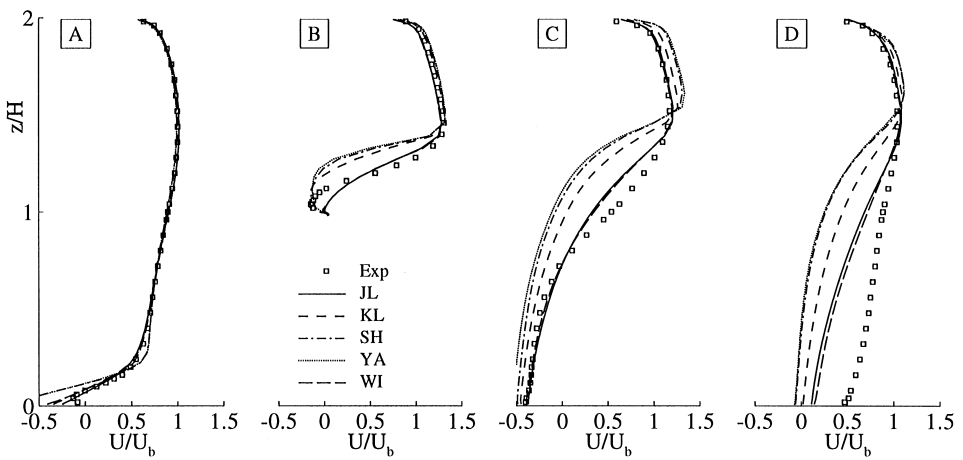

Fig. 4. Mean velocity in the vertical plane of symmetry along the main flow direction.

in the impingement region therefore leads to worse results in the wake region for the type of flow considered in the present study. The results of the WI model ($X_R/H = 2.31$) are closest to the experimental results ($X_R/H = 1.66$). All turbulence models predict the height of the forward stagnation point Z_S/H very well (see Table 2).

Fig. 4 shows calculated mean velocity profiles in the vertical plane of symmetry of the cube along the main flow direction for four different locations given in Fig. 3. The height z and the velocity U are nondimensionalized with the cube height H and the bulk velocity U_b, respectively. Square symbols indicate the experimental results from Martinuzzi and Tropea [19]. In front of the cube (Position A) all model results agree very well with the experimental results except for the region close to the ground. The difference in this region indicates that the size of the predicted horse-shoe vortex differs from the measured one (see also Table 2). As already mentioned the separation bubble on top of the cube (Position B) predicted by the WI model is clearly too small whereas the bubble predicted by the YA and SH models is too large. Downwind of the cube at position D both the JL and the WI model outperform the other

investigated models. Further downstream the predicted recirculation region is too large indicating that the performance of all models degrades due to highly anisotropic turbulence.

4.2. Flow and dispersion in the vicinity of a U-shaped building

The microscale model MIMO was employed to investigate the dispersion of a passive pollutant in the vicinity of a U-shaped building. Detailed measurements for this configuration were carried out in a wind tunnel (Klein et al. [20]). The wind tunnel model corresponded to a real building which is 52 m wide, 40 m deep and 28 m high. The wings of the building were 12 m wide. Simulations were carried out for several wind directions and emission source locations. In this paper the results for one wind direction are shown (see Fig. 5). A statistical evaluation is given by Götting et al. [21]. The atmosphere was assumed to be neutrally stratified. The velocity profile at the inflow boundary was adapted to the power law given by Eq. (6) with the exponent $\alpha = 0.28$. The reference velocity U_r was equal to 5 m/s at the reference height $z_r = 10$ m. The turbulent flow was simulated using the JL turbulence model.

Velocity vectors in a horizontal cross section 10 m above the ground are shown on the left hand side of Fig. 6. They reveal the complex vortex structures around the building. For the investigation of the dispersion of pollutants a source was located in the center of the courtyard 2 m above the ground (location *B* in Fig. 5). The source was assumed to be non-buoyant and with negligible initial momentum. Fig. 6 (right) shows a vertical cross section through the concentration field at a distance 40 m downwind of the reference point. The cross section indicated by a dashed line in Fig. 5 is

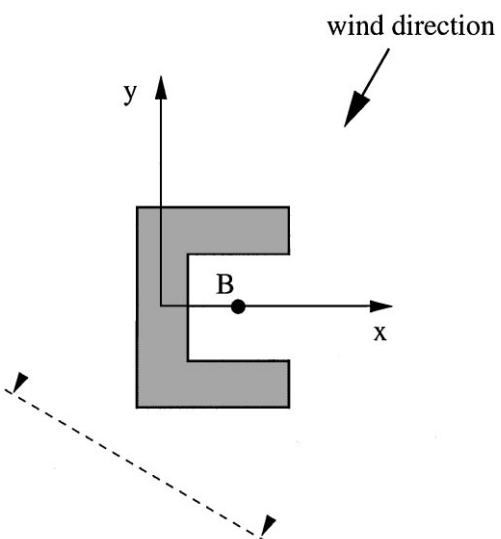

Fig. 5. Sketch of the investigated U-shaped building and location of the vertical slices.

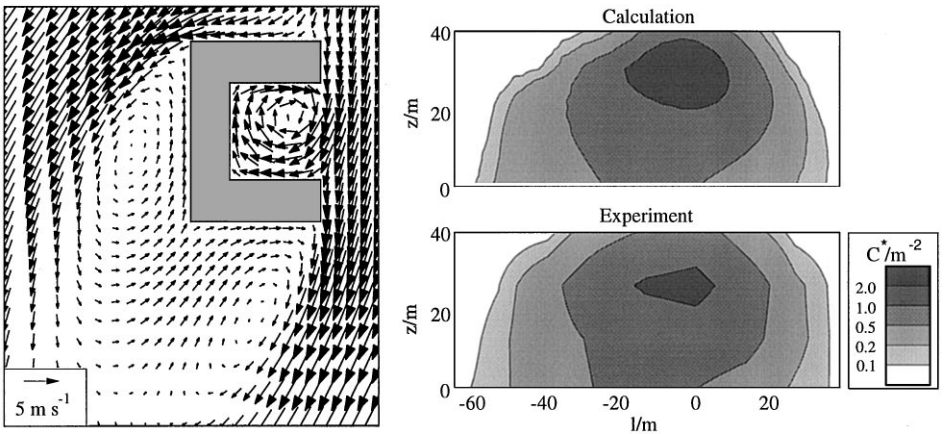

Fig. 6. Flow field 10 m above ground level and vertical slices (location see Fig. 5) of the concentration of a passive pollutant in the vicinity of a U-shaped building.

perpendicular to the main wind direction. Concentrations C are normalized with the source strength $\dot{Q}$ and the reference velocity U_r, according to

$$C^{\star} = 10^3 \cdot C \cdot U_r / \dot{Q}.$$

The calculated concentrations agree very well with the measured concentrations. Further investigations showed that the overall structure of the predicted plume is in good agreement with the measurements. The locations of local maxima are also predicted well indicating that the numerical model determines the average flow field well.

4.3. *Wind flow over an industrial area*

The coupled system MEMO-MIMO was applied to an industrial area in south-western Germany, namely a part of the BASF site near the greater urban area of Mannheim and Ludwigshafen. These cities are located in the northern part of Baden-Württemberg where the river Neckar joins the river Rhine. The Rhine valley is bordered by the hills of the Odenwald and the Pfälzer Wald. North of the cities are the Taunus and the Spessart. The coupled model was chosen to take influences of these mountains on the local wind flow into account and to provide realistic boundary conditions for the microscale simulation. The buildings considered in the microscale simulations and the measuring stations (indicated by squares) are shown in Fig. 7.

Table 3 shows the measured and the predicted microscale wind speed and wind direction. The measured values are annual averages of the results from the measuring stations shown in Fig. 7. For the simulation a meteorological situation was chosen which corresponds to the mean yearly wind flow. Microscale quasi-steady flow fields were calculated for four characteristic times of the day: morning (9 am), noon,

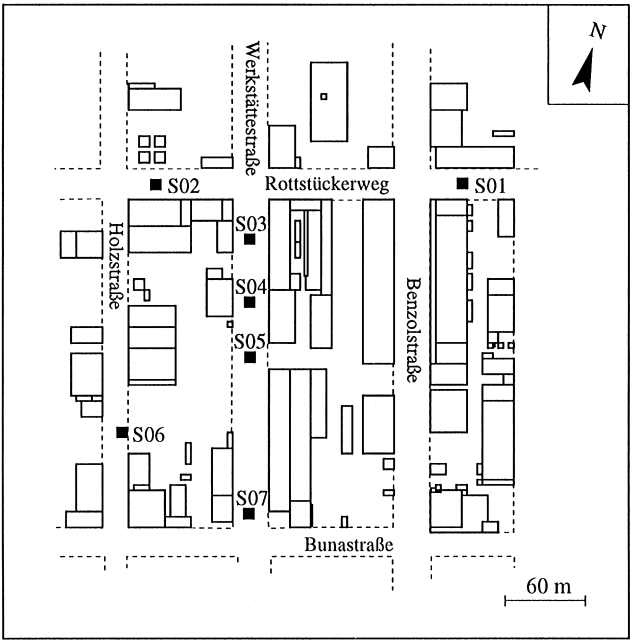

Fig. 7. Sketch of the investigated domain and locations of the measuring stations (S01–S07).

Table 3
Comparison between measurements and numerical simulation

	Measurements		Simulation	
Station	$\bar{u}$/m s^{-1}	φ/°	$\bar{u}$/m s^{-1}	φ/°
S01	0.93	248–275	1.29	254–268
S02	1.03	256–284	1.28	234–258
S03	1.29	140–178	1.79	151–169
S04	1.28	130–175	1.74	148–169
S05	1.33	165–250	1.70	160–196
S06	1.70	175–202	2.07	186–197
S07	1.72	150–250	2.36	205–234

afternoon (3 pm) and night (9 pm). The values given in Table 3 are averaged over these four characteristic times.

The wind speed is slightly overestimated by the numerical model because the modeling domain covers only a sector of the industrial site. Hence, the deceleration by the buildings is underestimated by the model. At the stations *S*06 and *S*07 the wind speed is higher compared to the other stations. The main wind flow is approaching

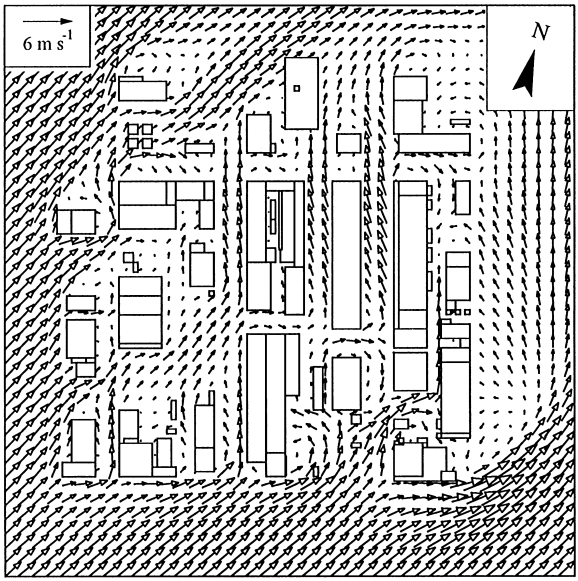

Fig. 8. Flow field 5 m above the ground level.

from south-westerly directions. The stations *S*06 and *S*07 are at the south-western boundaries where the inflow is nearly unaffected by the buildings. This can also be observed from the velocity vectors in a horizontal cross section 5 m above the ground shown in Fig. 8.

Comparisons of measured and predicted results showed a good agreement indicating the plausibility of the model results. Due to the coupling procedure realistic initial and boundary values for the microscale simulations have been generated without having detailed measurements of the wind flow in the surroundings. Therefore, the capability of the model to reliably predict the wind flow in built-up areas even in a complex orography was emphasized.

5. Conclusions

An overview of the capabilities and features of the microscale model MIMO has been presented. The model MIMO comprises solution procedures for the transport equations momentum and scalars. It is suited for the prediction of flow fields and plume dispersion in microscale domains. Several cases, e.g., the flow over a surface mounted cube and the flow in the vicinity of a U-shaped building, which have been employed for the validation of the numerical model indicate the applicability of the numerical model. Further simulations for complex building structures indicate the capabilities of the model to predict wind flow and pollutant dispersion also for realistic applications.

Acknowledgements

The partial support for this work from the Deutsche Forschungsgemeinschaft is gratefully acknowledged.

References

[1] C. Winkler, Mathematische Modellierung der quellnahen Ausbreitung von Emissionen, Fortschritt-Berichte VDI, Reihe, Vol. 7 (268), VDI-Verlag, Düsseldorf, Germany, 1995.
[2] T. Flassak, Ein nicht-hydrostatisches Modell zur Berechnung der Dynamik der planetaren Grenzschicht, Fortschritt-Berichte VDI, Reihe, Vol. 15 (74), VDI-Verlag, Düsseldorf, Germany, 1990.
[3] N. Moussiopoulos, Mathematische Modellierung mesoskaliger Ausbreitung in der Atmosphäre, Fortschritt-Berichte VDI, Reihe, Vol. 15 (64), VDI-Verlag, Düsseldorf, Germany, 1989.
[4] O. Reynolds, On the dynamical theory of incompressible viscous fluid and the determination of the criterion, Philos. Trans. Roy. Soc. London, Series A 186 (1895) 123–164.
[5] W.P. Jones, B.E. Launder, The prediction of laminarization with a two-equation model of turbulence, Int. J. Heat Mass Transfer 15 (1972) 301–314.
[6] M. Kato, B.E. Launder, The modelling of turbulent flow around stationary and vibrating square cylinders, Proceedings of the 9th Symposium on Turb. Shear Flows, Kyoto, Japan, 1993.
[7] T.-H. Shih, W.W. Liou, A. Shabbir, Z. Yang, J. Zhu, A new k–ε model for high reynolds number turbulent flows, Comput. Fluids 24 (1995) 227–238.
[8] V. Yakhot, S.A. Orszag, S. Thangam, T.B. Gatski, C.G. Speziale, Development of turbulence models for shear flows by a double expansion technique, Phys. Fluids A 4 (1992) 1510–1520.
[9] D.C. Wilcox, Reassessment of the scale-determining equation for advanced turbulence Models, AIAA J. 26 (1988) 1299–1310.
[10] U. Schumann, H. Volkert, Three-dimensional mass- and momentum-consistent Helmholtz-equation in terrain-following coordinates, In: Hackbusch, W. (Ed.), Notes on Numerical Fluid Mechanics, Vol. 10, Vieweg Verlag, Braunschweig, Germany, 1984, pp. 109–131.
[11] T. Flassak, N. Moussiopoulos, An application of an efficient non-hydrostatic mesoscale model, Boundary-Layer Meteorol. 41 (1987) 135–147.
[12] A. Harten, On a large time-step high resolution scheme, Math. Comput. 46 (1986) 379–399.
[13] M. Wortmann-Vierthaler, N. Moussiopoulos, Numerical tests of a refined flux corrected transport advection scheme, Environ. Software 10 (1995) 157–176.
[14] B.E. Launder, D.B. Spalding, The numerical computation of turbulent flows, Comput. Meth. Appl. Mech. Eng. 27 (1974) 1485–1984.
[15] I.A. Khatib, Verfahren zur Verknüpfung von mesoskaligen und mikroskaligen Modellen der atmosphärischen Grenzschicht, Fortschritt-Berichte VDI, Reihe, Vol. 15 (205), VDI-Verlag, Düsseldorf, Germany, 1998.
[16] D. Carson, P. Richards, Modelling surface turbulent fluxes in stable conditions, Boundary-Layer Meteorol. 14 (1978) 67–81.
[17] B. Hicks, Windprofile relationships from the Wangara experiment, Quart. J Roy. Meteorol. Soc. 96 (1976) 535–551.
[18] K.M. Carpenter, Note on the paper 'Radiational condition for the lateral boundaries of limited-area numerical models' by M.J. Miller, A.J. Thorpe, Quart. J. Roy. Meteorol. Soc. 108 (1998) 717–719.
[19] R. Martinuzzi, C. Tropea, The flow around surface-mounted, prismatic obstacles placed in a developed channel flow, J. Fluids Eng. 115 (1993) 85–92.
[20] P. Klein, M. Rau, Z. Wang, E. Plate, Concentrations and flow field in the neighbourhood of buildings and building complexes (wind tunnel experiments), Annual Report 1995, Research Programme for Air Pollution Prevention Measures, Forschungszentrum Karlsruhe, Germany.
[21] J. Götting, C. Winkler, M. Rau, N. Moussiopoulos, G. Ernst, Dispersion of a passive pollutant in the vicinity of a U-shaped building, Int. J. Environ. Poll. 8 (1997) 718–726.